Contributed paper

OPTO-ELECTRONICS REVIEW 8(1), 43–55 (2000)

$Al_xGa_{1-x}N$ based UV visible-blind photodetector device applications

F. OMNES[1*], E. MONROY[2], F. CALLE[2], E. MUÑOZ[2], B. BEAUMONT[1], and P. GIBART[1]

[1]CNRS-CRHEA, rue Bernard Grégory, Sophia-Antipolis F-06560 Valbonne, France
[2]Departamento de Ingenieria Electronica – Universidad Politécnica de Madrid – Ciudad Universitaria s/n 28040 Madrid, Spain

$Al_xGa_{1-x}N$ material system whose bandgap lies in the 3.42–6.2 eV range is extremely interesting for visible and solar blind UV photodetector applications. This paper describes the device performances of $Al_xGa_{1-x}N$ (x = 0–35%) UV photoconductors and Schottky barrier photodetectors for visible- visible-blind appplications grown on c-oriented sapphire, with a detailed balance with the basic materials properties. Conventional low-temperature grown AlN or GaN were used for all applications. High quality Schottky barrier photodiodes made of epitaxial lateral overgrown (ELOG) GaN are also presented. All Schottky barrier devices show a fast time response (15 ns for $Al_{0.22}Ga_{0.78}N$(Si) photodiodes grown on AlN nucleation layers), a high UV-visible rejection factor (> 3 orders of magnitude for AlGaN(Si) photodiodes grown on GaN or AlN nucleation layers, and rising up to 4 orders of magnitude for the GaN ELOG material), and high absolute values of above bandgap reponsivities (up to 130 mA/W for GaN ELOG materials). New application of AlGaN UV Schottky barrier photodetectors to monitor the biological action of the solar UV radiation as well as the device performance of high quality GaN and AlGaN metal semiconductor metal with cutoff wavelengths as short as 310 nm, are described in detail.

Keywords: ultraviolet detectors, photoconductors, photodiodes, Schottky barrier photodiodes, MSM detectors.

1. Introduction

The material properties of hexagonal III-nitride semiconductors grown on substrates like c-oriented sapphire or SiC make them of a very special interest to optotelectronic and electronic device applications. A new generation of light emitting devices, photodetectors and field effect transistors is nowadays emerging using these materials. InGaN/GaN blue to green light emitting diodes have been extensively developed worldwide by several companies (Nichia Chemical Industries, Cree Research, Osram Opto Semiconductors, Hewlett Packard, Toyoda Gosei, etc.) and they are already commercially available. The most recent improvement in the GaN nucleation techniques on sapphire [epitaxial lateral overgrowth (ELOG)], which thoroughly reduces the total dislocation density in the GaN-based materials, now leads to the fabrication of InGaN/GaN blue laser diodes working in room-temperature continuous-wave operation with lifetimes beyond 10,000 hours [1]. GaN and AlGaN-based ultraviolet photodetectors are now commercially available (APA Optics) for visible blind applications. The earliest junction-based nitride photodetectors reported are p-type GaN-based Schottky barrier photodiodes with a Ti Schottky contact [2]. GaN photovoltaic diodes have proved on their own to be a very competitive approach in applications requiring speed or a high UV/visible contrast [3]. GaN and $Al_xGa_{1-x}N$-based photoconductors [4–7], Schottky barrier photodiodes [8–10], metal-semiconductor-metal photodetectors [11–13], and p-i-n photodiodes [14–17] have been demonstrated with good operating characteristics. Applications for GaN Schottky photodiodes have been found for visible-blind imaging and solar UV detection instruments [3]. A visible-blind imaging system using a 32×32 array of p-i-n GaN/AlGaN photodiodes with a high detectivity has also been very recently reported [18].

In this paper, we will concentrate on the use of III-Nitride materials for visible-blind UV photodetector device applications. We will first develop the MOVPE growth of $Al_xGa_{1-x}N$ alloys, focusing on their typical structural, optical and electrical properties. Some realisations in the field of ultraviolet $Al_xGa_{1-x}N$-based photodetectors will be described in detail.

2. Material properties of III-nitrides grown on sapphire

Hexagonal III-nitride compounds are mostly interesting for their optoelectronic applications, as they considerably extend the spectral limits towards higher energies in light emitting devices and photodetectors with respect to classical semiconductors (Si, GaAs, GaP, InP and related compounds). The first feature of III-nitride alloys is obviously

*e-mail: fo@crhea.cnrs.fr

their wide bandgap energy, which is 3.42 eV for GaN at room temperature, lies in the 1.9–3.42 eV range for $In_{1-x}Ga_xN$ (x = 0–1), and reaches the 3.42–6.2 eV range for $Al_xGa_{1-x}N$ alloys (x = 0–1). Direct bandgaps are obtained in the full compositional range of InGaN and AlGaN ternary alloys, which make them fully useable in the whole set of optoelectronic applications such as amber red, purplish, green, blue, and UV light emitting devices (InGaN/GaN based light emitting diodes, laser diodes) or UV photodetectors (AlGaN based photoconductors, Schottky photodiodes, and p-i-n photodiodes).

Visible-blind UV photodetectors are of a great interest mainly because of their numerous applications such as UV-B monitoring, flame detection or UV dosimetry. Due to the high visible or infrared spectral response of Si or other narrow-bandgap III-V compound semiconductors, their setup for visible-blind UV photodetection requires tuned high-pass absorbant filters, and sometimes even luminescent filters which selectively absorb the UV radiation and reemit light with a photon energy very close to the bandgap value of the active semiconductor [19]. This limitation results in quite large, complicated and expensive instruments, which most often have reliability limited in time due to the ageing of the filters. The high bandgap values of GaN or AlGaN materials allows the fabrication of UV photodetectors without any filter, as the device can be directly illuminated by the UV radiation without displaying any visible or infrared-related photoresponse [20]. Minaturised, reliable, and low cost UV photodetectors can thus be obtained with stable performances. Furthermore, high UV to visible contrasts, beyond 3 orders of magnitude, is a very common feature in the spectral response of Schottky barrier, p-i-n and MSM GaN and AlGaN-based photodetectors, together with low noise and fast time responses typically lying in the nanosecond scale.

As free-standing bulk monocrystalline gallium nitride is not available with a sufficient size and crystal quality, there is a lack of a lattice matched substrate for the growth of gallium nitride. C-oriented sapphire is therefore the most commonly used substrate in the MOVPE process, despite its large lattice mismatch (about 16%) with GaN. However, the direct growth of gallium nitride on the basal plane of sapphire usually drives to a poor quality, polycrystalline material unusable for device applications. One good way to grow a monocrystalline GaN material with fair structural properties uses a thin, low temperature grown 25-nm thick GaN [21] or 10-nm thick AlN [22,23] nucleation layer between the sapphire substrate and the main GaN epilayer.

The best structural and optical properties of AlGaN on GaN and AlN nucleation layers are obtained for x lying in the 0.10–0.35 range using pure hydrogen as a carrier gas and growth temperatures which are typically 20–40°C higher than the growth temperatures currently used for GaN. Interestingly, the optimal growth temperature window for AlGaN alloys seems to be narrow, and changes in the growth temperature as small as 10°C give large differences in the structural properties, such as the surface morphology, especially at growth temperatures higher than 1150°C. Also, in the case of AlGaN alloys with aluminium contents higher than 20% in the solid phase, the growth temperature has to be re-adjusted to 1180°C, as a significantly rougher surface morphology is obtained at a growth temperature of 1170°C. LP-MOVPE growth conditions of AlGaN on c-oriented sapphire substrates over GaN or AlN nucleation layers are summarised in Table 1.

The x value in $Al_xGa_{1-x}N$ is determined by energy dispersion spectroscopy (EDS). Pure Ga and Al standards are used for calibration in the scanning electron microscope in order to get an optimal accuracy and reliability of the EDS measurements.

Mirror-like surface morphologies of $Al_xGa_{1-x}N$ epilayers directly grown on GaN and AlN nucleation layers are obtained for all aluminium compositions, for x lying in the 0–0.35 range. A typical full width at half maximum (FWHM) of 670 arc-seconds is measured for the (0002) diffraction peak in the ω-configuration for $Al_{0.10}Ga_{0.90}N$ epilayers grown on c-oriented sapphire. For higher values of the aluminium concentration (up to 0.35), this value doesn't exceed 800 arc-sec. A clear illustration of fair structural properties of AlGaN materials can also be given by θ/2θ X-ray diffraction patterns of AlGaN/GaN heterostructures (Fig. 1).

Cross-section transmission electron microscope (TEM) performed on AlGaN epilayers concluded to the presence

Table 1. LP-MOVPE growth conditions of AlGaN (process data are given for an AIX 200 RF LP-horizontal MOVPE equipment).

III elements	Trimethylaluminium, Trimethylgallium
Nitrogen source	Ammonia, purified
Carrier gas	Pure H_2
Total flow in growth chamber	4.5 l/min
Growth pressure	50 hPa
Ammonia flow	2 l/min
V/III ratio	3500
Growth temperature	1170°C (x < 20%) – 1180°C (higher Al compositions)
Growth rate	About 1 μm/h (depending on the Al composition)

 © 2000 COSiW SEP, Warsaw

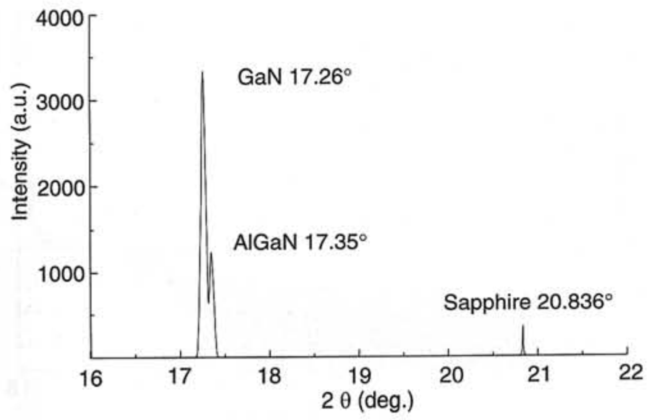

Fig. 1. X-ray θ/2θ double diffraction pattern of a 700 nm $Al_{0.1}Ga_{0.9}N$/2-μm GaN heterostructure grown on c-oriented sapphire with a GaN nucleation layer.

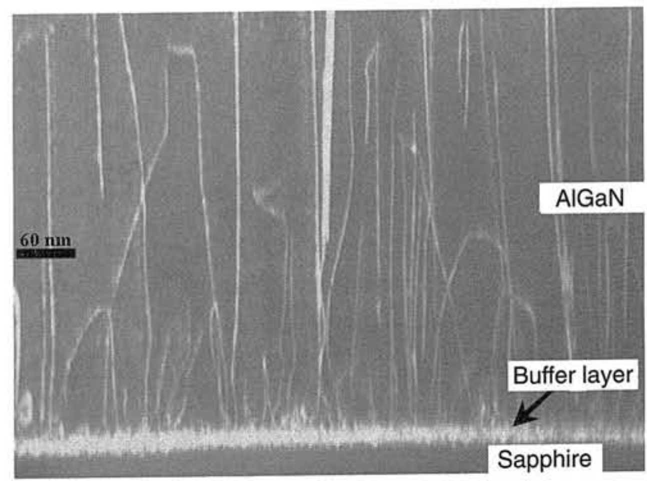

Fig. 2. Cross-sectional TEM picture of an $Al_{0.15}Ga_{0.85}N$ epilayer grown on c-oriented sapphire using an AlN nucleation layer.

of **c-** and **a+c-** dislocations (Fig. 2). The interface with the sapphire substrate is highly defective, with a typical spatial extension of a few tens nanometers (60 nm in the case of Fig. 2) in the c-direction. It is interesting to note that most of the dislocations are in the form of dislocation loops located close to the substrate-epilayer interface region, which never reach the semiconductor surface.

Optical properties of non intentionally doped AlGaN epilayers with various aluminium compositions lying in the 0–35% range grown on AlN or GaN nucleation layers have been investigated. Figure 3 displays typical T = 300 K photothermal deflection spectrocopy (PDS) patterns measured on $Al_xGa_{1-x}N$ epilayers with various aluminium concentrations lying in the 0–35% range, grown on a non- -absorbant AlN nucleation layer. The main feature of all these absorption spectra is a sharp transition in the absorption coefficient for photon energies close to the value of the energy gap, giving a clear evidence of the optical quality of the AlGaN layers with a low concentration of deep energy levels.

The variation of the T = 300 K energy gap E_g as a function of the aluminium concentration x in the solid phase can be fitted by the relationship:

$$E_g = 3.43(1-x) + 6.12x - b.x(1-x)$$

with a value of the bowing parameter value, b, of 0.8(±0.1) eV (Fig. 4), lying between the two extrema of the previously determined values: b = –1 [24], and b = 1.3 eV [25] or even 1.33 eV [26]. It must be noted that a zero value of the bowing parameter has been recently determined by Ochalski *et al.* [27], in accordance with two previous works [28,29]. Our experimental value is close to the 0.62(±0.45) eV bowing parameter very recently reported by Lee *et al.* [30].

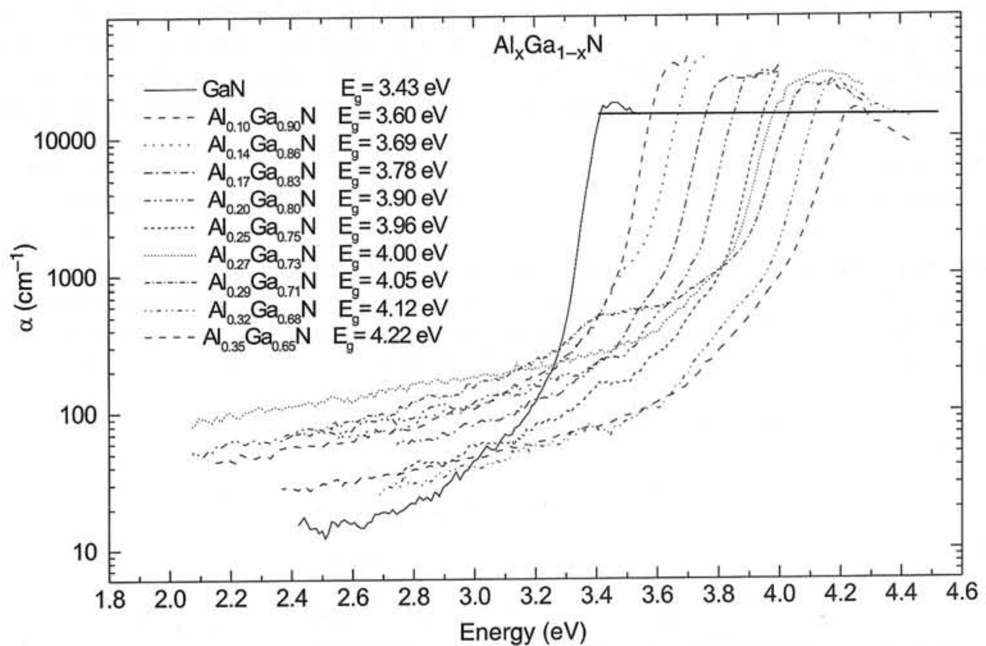

Fig. 3. AlGaN grown on AlN nucleation layers. Absorption coefficient deduced from PDS measurements at T = 300 K.

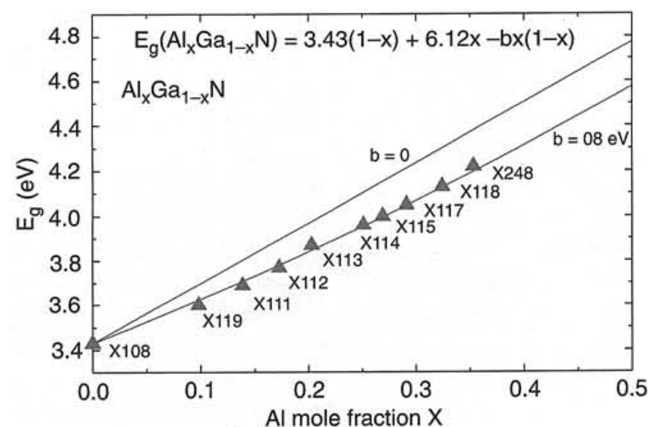

Fig. 4. Variation of the energy gap at T = 300 K for AlGaN samples grown on AlN nucleation layers (measured by PDS) as a function of the aluminium fraction in the solid phase (measured by calibrated EDS).

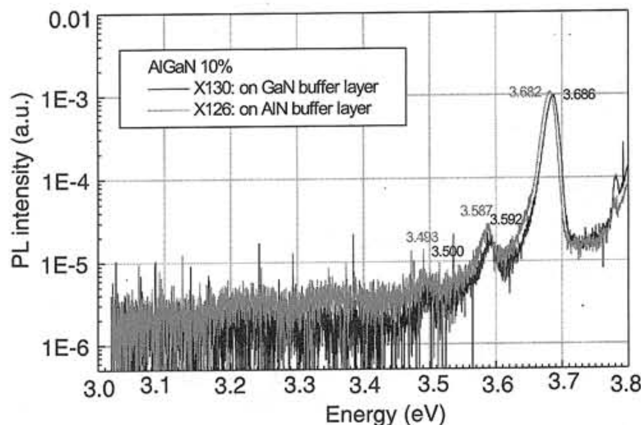

Fig. 5. Low temperature photoluminescence measurements on non-intentionally doped AlGaN epilayers with an aluminium content of 10%, grown on GaN and AlN nucleation layers (T = 9 K, He-Cd laser excitation).

As a conclusion, it is important to outline that we find this special feature independent on the chemical nature of the nucleation layer, as no significant difference is observed in the energy gap of AlGaN layers grown on GaN and AlN nucleation layers at a given value of the aluminium concentration.

In order to better determine the optical properties of AlGaN epilayers, low temperature photoluminescence has been performed at T = 9 K using a He-Cd laser working at a wavelength of 325 nm. The corresponding photon energy is about 3.8 eV, which is high enough to get the excitation of AlGaN with aluminium concentrations lower than 17%. It has been then possible to look for the low temperature photoluminescence properties of AlGaN with respective aluminium contents up to 14%.

In Fig. 5, the T = 9 K PL spectra of two AlGaN epilayers with an aluminium content of 10% are plotted together. These layers were respectively grown on GaN and AlN nucleation layers under similar growth conditions. Identical optical properties can be observed on both layers. Also, the photon energies of the optical transitions are almost the same in both cases, thus assessing the reproducibility of the growth conditions of the layers. The near-edge excitonic peak (most likely donor-bound exciton) is located at 3.685 eV, followed by 2 phonon replica (the photon energy separation between two adjacent peaks is constant and equal to 94 meV). The full width at half maximum of the main photoluminescence peak is 18 meV in both cases, comparable to other state-of-the art values already published for AlGaN [31,32]. All these features are highly representative of the quality of the AlGaN epilayers, which appears to be very similar on both GaN and AlN nucleation layers taking low temperature photoluminescence data as references. It is important to note that no low energy radiative transitions related to residual acceptors were observed in the 3.2–3.4 eV range.

The electrical properties of n-type doped GaN and AlGaN were measured by Hall effect at room temperature (T = 300 K) using indium-based ohmic contacts. 1 μm-thick silicon-doped GaN and AlGaN n-type epilayers were grown on GaN nucleation layers, with a typical doping level lying in the 5×10^{17}–2×10^{18} cm^{-3} range. Typical mobilities of 180 cm^2/Vs and 60 cm^2/Vs were respectively measured on GaN and AlGaN with aluminium contents lying in the full 10–35% range (Table 2). It is interesting to note that room temperature mobility of 330 cm^2/Vs are determined on a 0.2 μm-thick GaN(Si) epilayer for MESFET application, with a doping level of 5×10^{17} cm^{-3} grown on top of a 3-μm thick semi-insulating GaN buffer layer on a c-oriented sapphire substrate using a 250 Å-thick nucleation layer.

Epitaxial lateral overgrowth (ELOG) is a promising technique to achieve quasi defect-free GaN. ELOG technique consists in growing GaN on a pattern of windows opened by photolithography in a dielectric layer (SiO_2, Si_3N_4) deposited on a GaN layer grown on sapphire or SiC. GaN nucleates in the windows and grows laterally, so that the propagation of threading dislocations is avoided over the

Table 2. Hall effect measurements on GaN and AlGaN epilayers on sapphire (T = 300 K).

	GaN	GaN MESFET (0.2 μm GaN(Si)/3 μm GaN n.i.d.)	AlGaN 10–35%
Dopant	Silicon	Silicon	Silicon
N_D–N_A	5×10^{17} cm^{-3}	5×10^{17} cm^{-3}	$(1–2)\times10^{18}$ cm^{-3}
Mobility (T = 300 K)	180 cm^2/Vs	330 cm^2/Vs	60 cm^2/Vs

 © 2000 COSiW SEP, Warsaw

masked area. Thus, a sequence of high quality material (over the mask) and highly dislocated material (over the mask windows) is obtained. Typical pattern consist of stripes, with a period of 10–20 µm. Therefore, a standard detector should cover both high quality and low quality material, so its characteristics would be an average of both.

An alternative to avoid the low quality regions over the openings of the mask is the two-step ELOG process. It starts by growing a non-intentionally doped (n.i.d.) GaN layer on c-sapphire by metalorganic vapor phase epitaxy. Growth details are given elsewhere [33]. After growth, a thin layer (20–30 Å) of Si_3N_4 is deposited *in situ*. A pattern of 5-µm wide, 5-µm spaced bands is defined by standard photolithography and reactive ion etching. These bands are aligned with the [10-10] direction of the GaN layer. Once patterned, the sample is put back into the growth chamber. During the first step, standard growth conditions for n.i.d. GaN layers are used. In the overgrown GaN, threading dislocations bend by 90°, and propagate horizontally until the coalescence boundary. Therefore, the density of threading dislocations is reduced, although there is a noticeable surface roughness. Planarisation is achieved in the second step by using Mg doping which favours lateral growth rate and reduces vertical growth rate [34]. This two-step process results in a reduced defect density not only over the masked area, but also over the openings of the mask. Defects are confined to the coalescence boundaries, which is an improvement over the standard ELOG technique. Once the planarization is completed, a (3–4)-µm thick n.i.d. GaN layer is grown on top, in order to avoid the deleterious effects in the spectral response of the detectors, due to absorption by Mg-related levels.

3. $Al_xGa_{1-x}N$ based photodetectors

Non intentionally doped and Silicon doped $Al_xGa_{1-x}N$ layers were grown in the purpose of UV photodetector applications on c-oriented sapphire substrates. Several kinds of photodetectors were fabricated:

- Photoconductors, using $Al_xGa_{1-x}N$(Si) epilayers grown in GaN or AlN nucleation layers.
- Schottky barrier photodiodes, using GaN and AlGaN(Si) epilayers grown on GaN or AlN nucleation layers, and GaN epilayers grown on ELOG GaN buffers.
- Metal semiconductor metal (MSM) photodetectors, using highly resistive, non intentionally doped $Al_xGa_{1-x}N$ epilayers.

The influence of the most important materials properties, such as crystalline defects or the room temperature persistent photoconductivity on the time response of photoconductors, as well as the effect of the nature of the nucleation process ("classical" GaN or AlN buffers, and ELOG materials) on the performances of GaN Schottky barrier photodiodes and the improvement in UV/visible contrast and responsivity on MSM photodetectors under the effect of bias, will be described in detail. A new application of AlGaN-based Schottky barrier photodiodes for the fabrication of a photodetector able to simulate the Commission Internationale de l'Eclairage (CIE) standard for the erythema sensitivity curve is also reported.

3.1. AlGaN photoconductors

Si-doped AlGaN samples of 2×4 mm² were used for photoconductors fabrication. Ti/Al ohmic contacts were deposited, leaving a free surface between contacts of about 1 mm². The polarisation circuit consists of a DC voltage source connected to the photoconductor in series with a small resistor. The photocurrent induced in the device is obtained from the variation of the voltage drop in the resistor under illumination conditions. In our system the bias voltage was held at 5 V. The responsivity was measured by exciting with a non-focused He-Cd laser (325 nm). Spectral response studies were performed using a 150 W Xe arc lamp with a Jobin-Yvon H25 monochromator. The optical system was calibrated with a Molectron PR200 pyroelectric detector.

3.1.1. Responsivity

GaN and AlGaN photoconductors show a DC responsivity that is highly dependent on incident power. It decreases approximately as $P^{-0.85}$, over five decades (see Fig. 6) [5,35]. This result is independent of the excitation wavelength, as shown in the inset of Fig. 6. An important decrease in responsivity with temperature has been also observed.

Figure 7 plots the spectral responsivity for photoconductors with different Al contents. The data are corrected to take into account the lamp response, considering the photocurrent dependence on the incident power analyzed above. The peak of the spectra is assigned to excitonic absorption. This peak shifts to shorter wavelengths when increasing Al content.

The UV/visible contrast in these devices is much lower than the one expected from the absorption coefficient of the

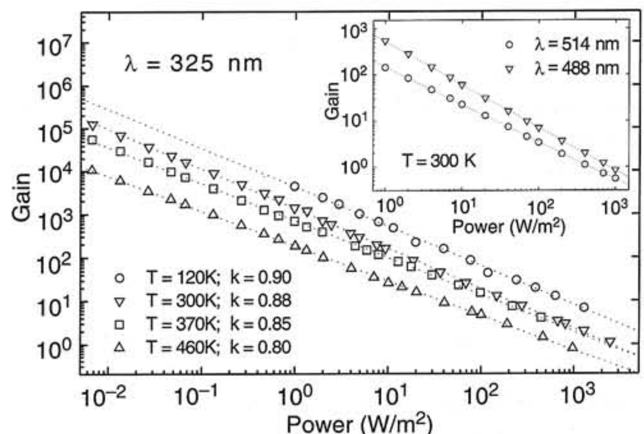

Fig. 6. Gain dependence on the incident optical power, measured in a GaN photoconductor at different temperatures.

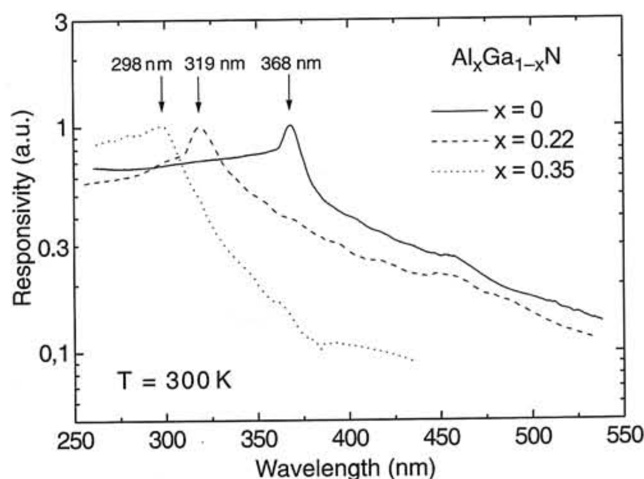

Fig. 7. Spectral response of AlGaN photoconductors with different Al contents and Si doping.

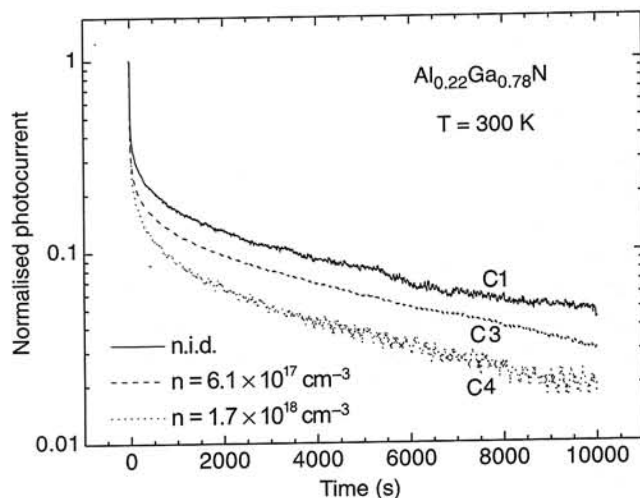

Fig. 8. Normalised photocurrent decays of $Al_{0.23}Ga_{0.77}N$ potoconductors, after an excitation light pulse from He-Cd laser.

material. Thus, the mechanism involved in the photoconductive responsivity cannot be only semiconductor optical absorption. This fact, together with the sublinear dependence of photocurrent on optical power, definitely supports the photoconductive mechanism described by Garrido *et al.* [36].

The conduction section does not correspond to the geometrical section of the devices, due to the presence of depletion regions around lattice discontinuities (threading dislocations, grain boundaries and interfaces). Charged regions around threading dislocations have recently been observed in GaN films by Hansen *et al.* [37] using scanning capacitance microscopy. Light induces a shrinking of these depletion regions, therefore modulating the conduction section.

This mechanism also explains the high response below the bandgap: the levels responsible for visible absorption can be due either to defects homogeneously distributed in the semiconductor, such as dopants or vacancies, or to defects localised in lattice discontinuities (dislocations, grain boundaries and interfaces). If charged, these defects originate a depletion region around them, reducing the effective conduction section of the device. Total light absorption by those defects may be negligible, so that they hardly affect the absorption coefficient and hence the photovoltaic detection. However, their effect on photoconductive responsivity is huge, since the charge concentrated in these discontinuities changes and thus modulates the effective conduction section.

3.1.2. Time response

All the samples showed persistent photoconductivity (PPC) effects. As shown in Fig. 8, the detectors show extremely slow and non-exponential transient responses, which are responsible for the frequency dependent responsivity observed by several groups [38–41].

Different explanations have been reported for PPC in GaN. Si or Mg has been proposed as the origin of PPC in doped samples [42,43], and oxygen contamination has also been suggested [44]. PPC has also been attributed to intrinsic material defects, such as Ga vacancies [45,46] or the defect responsible for the yellow photoluminescence emission [47,48].

Kung *et al.* [49] and Binet et al. [50] explain the non-exponential shape of the photocurrent decays with a model which assumes the presence of a trap level in the bandgap, ionised by the incident radiation. This model fits precisely the first milliseconds of the photocurrent decays and their dependence with the optical power [50], but it fails to explain the long non-exponential tails observed by most of the groups working with AlGaN photoconductors so far.

The slow photocurrent decays can be explained by recombination of electrons in the deep levels located at extended defects or dislocations [51]. In this process, the space charge region slowly recovers its width in the dark, and thus the resistance of the device also evolves slowly and non-exponentially towards its value in the dark.

3.1.3. Frequency modulation

Taking into account that the modulation of the conductive section is a very slow process, a possibility to improve the photoconductor spectral response consists in using a lock-in technique, which would eliminate all the phenomena occurring at slower rates than the chopping frequency. Another advantage of this measurement system is that the photocurrent obtained with a lock-in amplifier is quite independent of background current, as reported by Qiu *et al.* [45].
Figure 9 shows the responsivity dependence on the optical power for different chopping frequencies [52]. The responsivity becomes flatter when increasing the frequency from 7 Hz to 700 Hz, as the defect-related space charge regions involved in the DC photocurrent mechanism do not have enough time to react. For the same reason, the responsivity

 © 2000 COSiW SEP, Warsaw

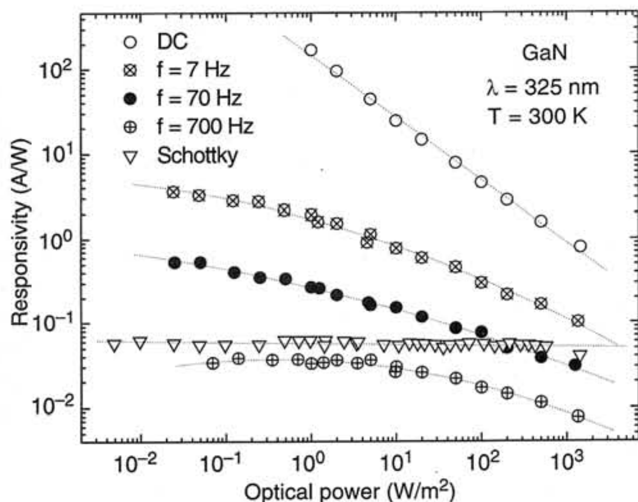

Fig. 9. Responsivity vs. optical power measured in a photoconductor using lock-in detection with different chopping frequencies. Data corresponding to a Schottky photodiode on the same sample is also presented for comparison.

decreases with frequency, as also observed by other groups [38,39,45,52].

The effect of the frequency on the photoconductive spectral response is depicted in Fig. 10 [7]. When the mechanism responsible for the PPC is reduced by increasing the chopping frequency, the cutoff becomes sharper and the spectrum below the bandgap tends to the photovoltaic response. However, the Schottky visible rejection remains much better than that of the photoconductor even for f = 700 Hz. In conclusion, their responsivity mechanism makes photoconductors unsuitable for applications requiring speed or a certain spectral contrast, unless lock-in detection is used. In this configuration, however, these devices lose all their advantages, since their responsivity is considerably reduced and the detection system becomes more complex and expensive.

3.2. AlGaN Schottky photodiodes

For the fabrication of planar Schottky barrier detectors, an extended Ti/Al ohmic contact was first deposited by e-beam evaporation. The Schottky contacts consist of semitransparent 10 nm thick Au disks, with a Ni/Au pad on top. Diode diameters ranged from $\phi = 200$ μm to $\phi = 1$ mm. Schottky barrier photodiodes are operated at zero-bias, and connected to a transimpedance amplifier with low input resistance (< 50 Ω) and a gain of 10^6 V/A.

In contrast with photoconductive detectors, Schottky barrier devices show a photocurrent that behaves linearly with incident power in the range measured (10 mW/m² to 2 kW/m²), as shown in the inset of Fig. 11. Figure 11 also plots the spectral responsivity of $Al_xGa_{1-x}N$ Schottky diodes with different Al contents (x = 0, 0.19, 0.26, 0.35). The cutoff wavelength shifts from 362 nm to 293 nm. A UV/visible contrast of more than three decades is obtained. Responsivity is quite flat for wavelengths higher than the bandgap, which is an advantage in comparison with GaN p-n junctions [10]. A slight decrease of the absolute responsivity has been observed with increasing Al content: absolute values of responsivities are 54, 45, 30 and 10 mA/W above the bandgap, for x = 0, 0.19, 0.26, and 0.35, respectively. A detailed comparison of the UV/visible contrast between photoconductors and Schottky photodiodes is shown in Ref. 7. The sharpness of the cutoff in Schottky barrier photodetectors indicates that the only limitation in the UV/visible contrast is given by the absorption in deep defects, in contrast with the results obtained in photoconductors.

The photodetector time response is limited by the RC-constant of the device, where C is the sum of the diode internal capacitance and the load capacitance, and R is the sum of the load resistance and the series resistance of the device. Therefore, the photocurrent decay time constant (time for the photocurrent to fall from maximum to 1/e) depends linearly on the load resistance, as shown in Fig. 12.

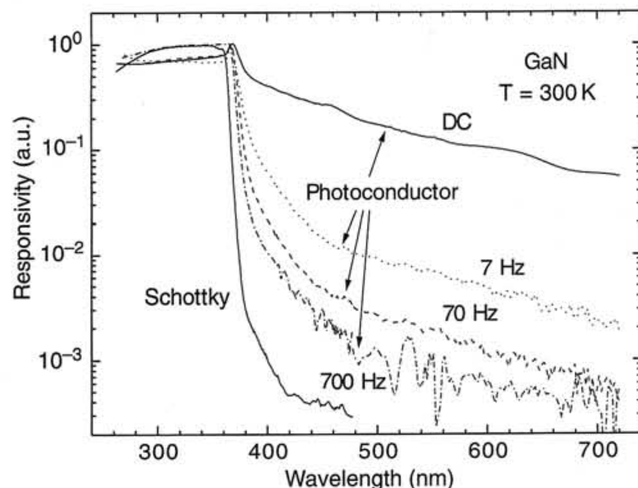

Fig. 10. Normalised spectral response of a photoconductor measured with the lock-in technique and different chopping frequencies. The spectrum of a Schottky diode on the same sample is also presented for comparison.

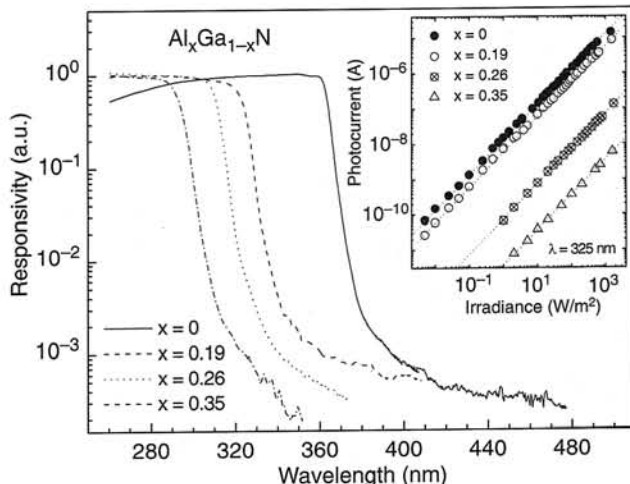

Fig. 11. Room temperature spectral response of AlGaN Schottly photodiodes with different Al contents. In the inset, variation of the photocurrent with optical power, measured with a He-Cd laser (λ = 325 nm).

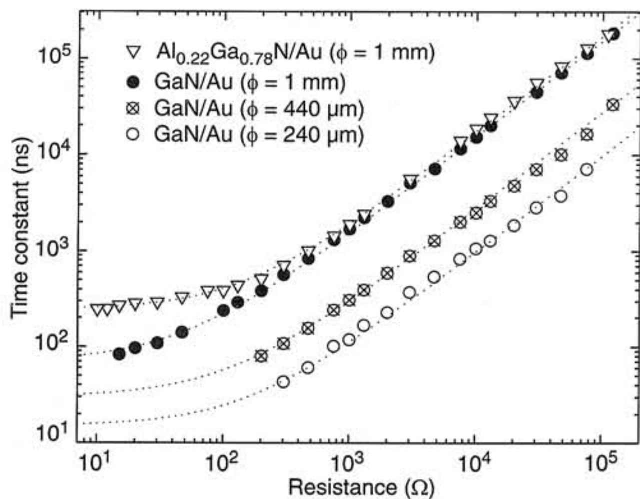

Fig. 12. Variation of the decay time constant with the load resistance, measured in AlGaN Schottky photodiodes with different sizes.

Minimum time constants of 69 ns have been recorded in diodes with a dimeter φ = 1 mm, going down to 15 ns for φ = 240 μm [10].

Detectivities of 6.1×10^9 cmHz$^{1/2}$W^{-1} and 1.2×10^9 cmHz$^{1/2}$W^{-1} have been reported respectively in GaN/Au and $Al_{0.22}Ga_{0.78}N$/Au Schottky photodiodes, at –2V bias [10].

3.3. Schottky barrier photodiodes fabricated on epitaxial lateral overgrown GaN

In spite of these promising characteristics, the heteroepitaxial growth of GaN results in a high dislocation density (~10^9 cm^{-2}), which limits the UV/visible contrast in GaN photodetectors. The recent development of ELOG GaN [53,54] has reduced the dislocation density for at least two orders of magnitude.

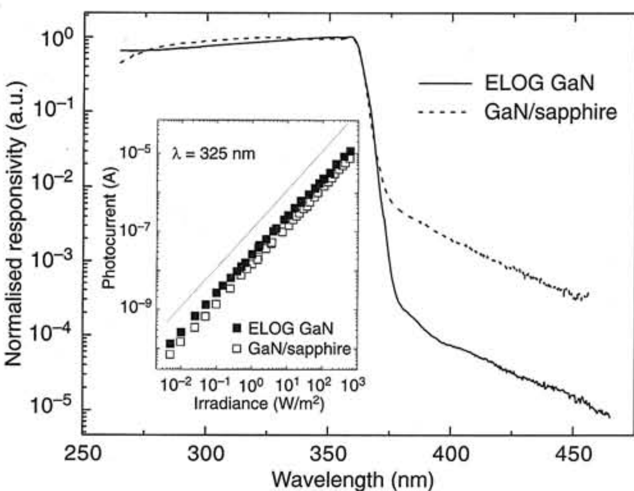

Fig. 13. Normalised spectral response of ELOG GaN Schottky photodiodes, compared with the spectral response of the same devices on standard GaN/sapphire. In the inset, photocurrent dependence on the optical power, measured with a He-Cd laser (325 nm).

Semitransparent Au Schottky barrier photodiodes have been fabricated on two-step ELOG GaN layers [55], showing a responsivity of 130 mA/W. An improvement in one order of magnitude in the UV/visible contrast has been observed, in comparison with devices on standard GaN on sapphire, as shown in Fig. 13. The leakage current is significantly reduced, below 1 nA/cm^2 at –1 V bias. The device time response is RC-limited, and the lower residual doping in these layers increases the bandwidth to over 30 MHz, 12 MHz, and 8 MHz in devices with a diameter of 200 μm, 400 μm, and 600 μm, respectively. Normalised detectivities as high as 5×10^{11} cmHz$^{1/2}$W^{-1} were measured at –3.4 V bias in Schottky photodiodes on two-step ELOG, with a diameter of 400 μm.

3.4. Application of AlGaN Schottky photodetectors for simulation of biological effects of UV radiation

UV radiation is able to produce a number of biological effects [56,59]:

- Pigmentation: maximum effect at 360–440 nm.
- Erythema (skin sunburn): maximum at $\lambda < 297$ nm.
- Synthesis of vitamin D_2 and D_3: 249–315 nm. Maximum at 290 nm.
- Plant damage: $\lambda < 317$ nm.
- Bactericidal radiation: 210–310 nm. Maximum at 254 nm.
- Carcinogenic radiation: UV-B and UV-C. Maximum at 310 nm.
- DNA damage: $\lambda < 320$ nm, increasing rapidly for shorter wavelengths.

Therefore, simple, accurate, reliable, low cost instruments are required to evaluate the biological effects of UV radiation. Broad-band UV detectors have been developed to fit the erythema action of the UV-A and UV-B wavelengths [58]. Commercial UV meters consist of narrow bandgap photodiodes (Si, GaAs, GaP), with a series of filters and phosphors in the optical path.

By using a certain Al mole fraction and proper growth conditions, Muñoz et al. [60,61] have demonstrated that the spectral response of AlGaN Schottky photodiodes can fit the erythema action spectrum, as shown in Fig. 14. Thus, the responsivity of these devices provides direct information on the biological effects of UV radiation. For this bio-effect application, AlGaN detectors now benefit from the absorption tails that are shown by state of the art AlGaN materials, response tails that allow to weight properly the lower UV-B band and the UV-A band to match the reference erythema action functions.

To monitor the solar UV-B radiation and the solar UV radiation effects, AlGaN photodiodes offer design flexibility, low cost, minimum size, and neither need for filters or coatings, nor for temperature stabilisation chambers. AlGaN detectors are adequate to perform both narrow-band

 © 2000 COSiW SEP, Warsaw

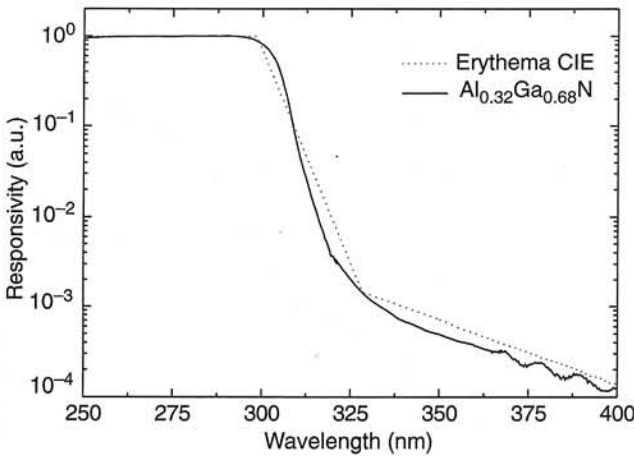

Fig. 14. Normalised spectral response of an AlGaN Schottky photodiode compared with the erythema action.

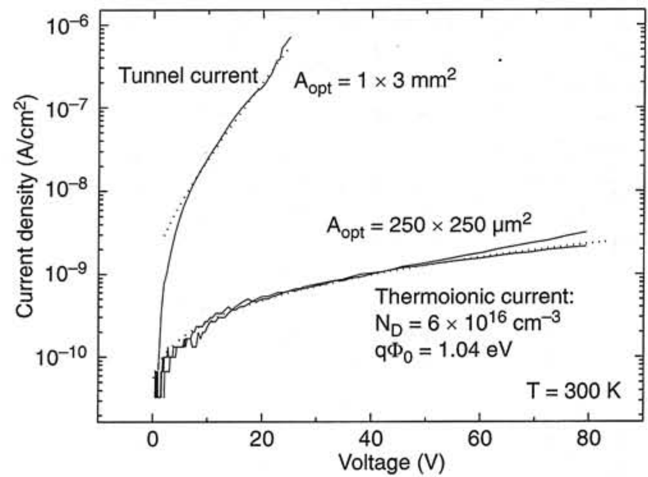

Fig. 15. Current-voltage characteristics of MSM photodiodes with different optical area, A_{opt}. Dotted lines correspond to fits assuming thermoionic emission transport and tunnel transport.

or broad-band irradiance measurements, and to monitor biological hazards. It is foreseen that these novel AlGaN UV detectors will definitively help to conduct environmental research in relation to ozone variations and UV radiation.

3.5. MSM photodiodes

MSM photodiodes consist in two interdigitated Schottky contacts on a planar surface [62,63]. These structures present some advantages over other photovoltaic detectors, like their fabrication simplicity, low dark current, low noise, high bandwidth capability, and suitability for integration with field effect transistors.

The devices were fabricated on 1.5-μm thick, n.i.d. $Al_xGa_{1-x}N$ ($0 \le x \le 0.25$) epilayers, grown by low-pressure metalorgarnic vapor phase epitaxy on c-sapphire. The layers were insulating. For the fabrication of Schottky barriers, samples were cleaned in HF:H_2O (1:10) and a Ni/Au bilayer (30 nm/100 nm) was deposited by Joule evaporation. The pattern of the metallisation was defined by a standard lift-off technique. The MSM structure consists of two interdigitated electrodes, with finger widths and gap spacings of 2, 4, and 7 μm, in an active area of 250×250 μm². Larger devices, with a finger width of 7 μm and a pitch of 12 μm, in an active area of 1×3 mm², have also been fabricated.

For their characterisation, the detectors were biased with a voltage source and connected in series with a transimpedance amplifier. Spectral responsivity studies were performed with a 150 W Xe arc lamp and a monochromator. The optical system was calibrated with a pyroelectric detector. The photodetector responsivity and its dependence on the optical power were determined by exciting with non-focused gas lasers (He-Cd, λ = 325 nm; Ar, λ = 257 nm, 458 nm, 488 nm, 514 nm). The response time of the detectors was measured using the fourth frequency of a Nd:YAG laser (266 nm), with 10 ns Gaussian pulses. Noise characterization was performed using a SR530 lock-in amplifier, the background noise power density of the system lying in the 10^{-26} A²/Hz range.

The detectors show a very low dark current density, which is indicative of high quality Schottky barriers and low defect density material. As shown in Fig. 15, the experimental current density of small devices fits quite well the thermoionic emission model for MSM structures, including the Schottky barrier lowering due to image force effects [64]. Considering the ideal GaN Richardson constant (A^* = 26 $Acm^{-2}K^{-2}$), a barrier height $q\Phi_0$ = 1.04 eV and a doping density N_D = 6×10^{16} cm^{-3} are obtained. Large area devices, in contrast, present an important tunnel transport contribution [13], as also shown in Fig. 15.

Figure 16 shows the spectral response of AlGaN MSM photodiodes at different bias. The responsivity is quite flat above the bandgap, with a sharp cutoff wavelength that shifts to shorter wavelengths with increasing Al content.

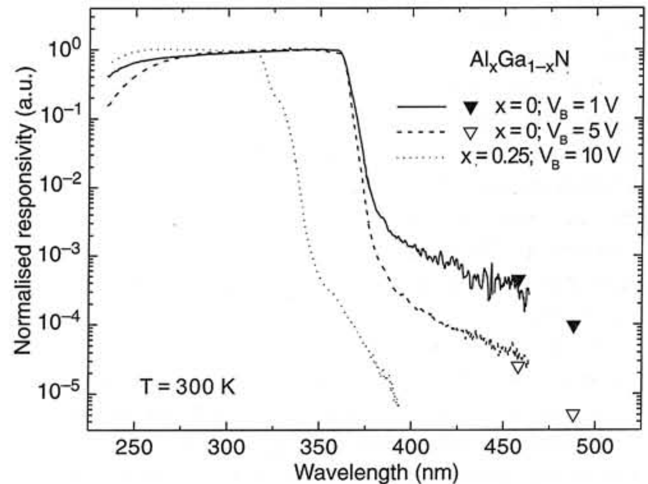

Fig. 16. Spectral response of AlGaN MSM photodiodes, measured under different bias. Triangles were obtained with the 458 nm and 488 nm lines of an Ar^+ laser.

A visible rejection of four to five orders of magnitude is obtained at 5 V and higher bias. However, the UV/visible contrast decreases by one decade when the bias is reduced from 5 V to 1 V, and remains at ~10^3 for lower bias [65]. The photocurrent scales approximately linearly with the optical power for wavelengths both over and below the bandgap, as seen in Fig. 17. This behavior is independent of bias.

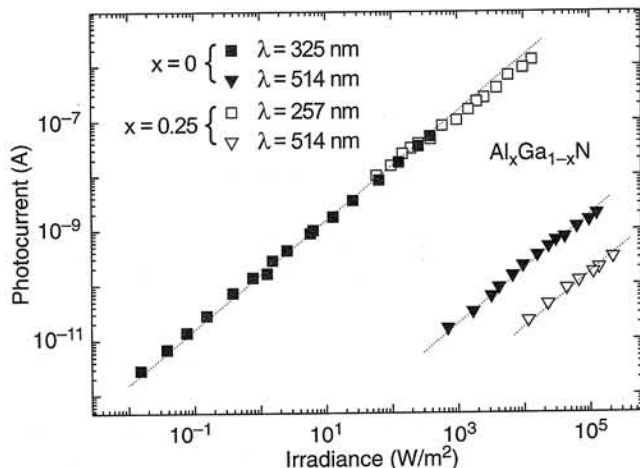

Fig. 17. Photocurrent vs. optical power in AlGaN MSM photodiodes for excitation both over and below the bandgap.

The variation of the responsivity with bias has been analyzed for diodes with different sizes, and excitation over the bandgap (see Fig. 18) [65]. For $V_B < 2$ V, the responsivity scales sublinearly with bias ($R \propto V_B^{0.7}$), which fits the theoretical behavior expected for an MSM photodiode in absence of gain, calculated from a one-dimensional model (dashed line in Fig. 18). An abrupt increase of the responsivity is observed between 2 V and 5 V, indicative of a bias-activated gain mechanism, which saturates for higher bias. This behaviour is independent of the finger width and the gap spacing, as also shown in Fig. 18.

The gain mechanism at high bias is also wavelength dependent, as shown in Fig. 19. For wavelengths longer than the bandgap, the device follows the trend expected for a MSM photodiode in absence of gain. The deviation from this behavior appears only for wavelengths shorter than 370 nm, so that the enhancement of the visible rejection with bias and the presence of gain are due to the same mechanism.

Gain in photodetectors is usually related to slow phenomena. Thus, the time response of these devices has also been analysed. The photocurrent decays are exponential, with time constants corresponding to the RC product of the measuring system, independently of bias. The variation of photocurrent response time with load resistance presents no trace of saturation for low load resistances. From these measurements, we can only conclude that the minimum response time of our devices is quite far below 10 ns. The

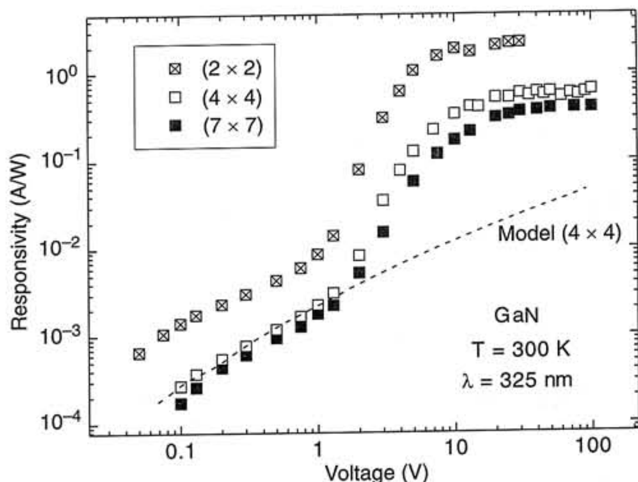

Fig. 18. Responsivity dependence on bias for and GaN MSM photodiodes, measured for excitation over the bandgap (325 nm), for various finger widths and gap spacings.

maximum bandwidth of the MSM photodiodes could be limited either by the RC product, where R is the load resistance and C the capacitance of the device, or by the carrier transit time of the detector, which are estimated in the picosecond range.

Given material data (doping concentration, barrier height) and the device geometry, the reach-through voltage of these MSM structures should be > 200 V, even for the devices with a pitch of 2 μm. Thus, most of the applied voltage drops in the reverse biased contact (cathode), and the photocurrent is produced by absorption in the cathode space charge region, with a small negative contribution by the anode. The higher responsivity observed in devices with a shorter gap spacing is not due to a more intense electric field, but to a higher number of fingers in the illuminated region. Therefore, responsivity saturation at high bias is not due to a full depletion of the device, but to gain saturation.

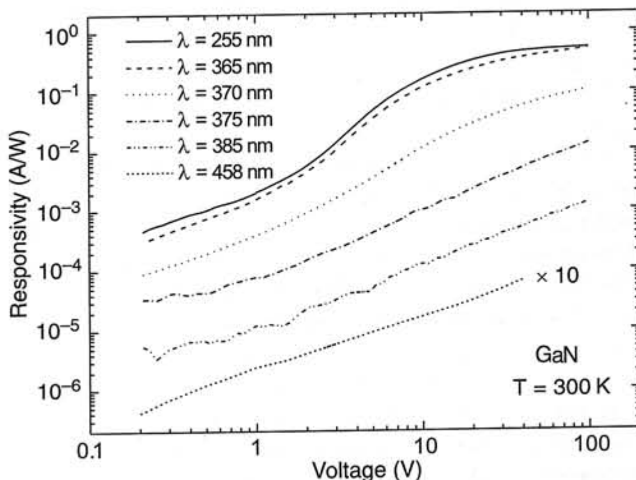

Fig. 19. Responsivity dependence on bias voltage, measured for different excitation wavelengths.

 © 2000 COSiW SEP, Warsaw

The gain mechanism observed is only active at bias higher than 2 V, and for excitation over the bandgap. This mechanism is responsible for the superlinear increase of the responsivity with bias [66,67] and the enhancement of the UV/visible contrast observed in AlGaN MSM photodiodes.

Gain in interdigitated MSM photodiodes has been reported and attributed to different mechanisms [68,70]. The most frequently suggested process consists in electron tunneling enhanced by whole accumulation at the cathode. This accumulation may be due to traps located either in the semiconductor surface, in the bulk material, or in a thin insulating layer between the metal and the semiconductor. Trapping at surface states or dislocations produces persistent photoconductivity effects and a sublinear behaviour with optical power, and degrades the spectral response of the devices. Both the linearity and the fast response of MSM photodiodes prove the absence of this gain mechanism, which is dominant in GaN and AlGaN photoconductors [7]. The presence of deep hole traps in bulk n.i.d. GaN is responsible for the photoresponse at excitation wavelengths longer than the bandgap, but the fact that gain is not observed for $\lambda > 370$ nm rules out trapping at these levels as the origin of this gain.

The increase in hole density in the vicinity of the cathode can also be explained by the difference in transit speeds between electrons and holes [68]. However, this phenomenon cannot justify either gain thatis only active for wavelengths over the bandgap. Finally, we can speculate about an avalanche process in the valence band as being responsible for the gain. At high bias, holes generated in the valence band near the cathode move towards the contact driven by the intense electric field, and might have enough energy to provoke new transitions by impact-ionisation.

Finally, the noise performance of the MSM devices was measured up to 28 V. At this bias, the spectral noise power of the GaN detectors remains always below the background noise level of the system, which implies a normalised noise equivalent power (NEP*) lower than 2 pW/Hz$^{1/2}$ in devices with finger width and gap spacings of 2 µm. At 28 V bias, a NEP* ~24 pW/Hz$^{1/2}$ was measured in $Al_{0.25}Ga_{0.75}N$ photodiodes [13].

4. Conclusions

A variety of $Al_xGa_{1-x}N$-based photodetectors (x = 0–0.35) have been fabricated and characterised, using AlGaN epilayers grown on GaN or AlN nucleation layers, or ELOG GaN.

AlGaN(Si)-based photoconductors showed a decreasing responsivity as a function of the incident optical power, approximately as $P^{-0.85}$. The spectral response of photoconductors displayed at all Al compositions (from x = 0 to x = 0.35) a peak related to excitonic absorption, which shifts to shorter wavelengths when increasing Al content. But slow and non-exponential transient responses were observed on all photoconductive devices. An improvement of the UV/visible contrast of photoconductors was observed as a function of the operating frequency, reaching 3 decades at a frequency of 700 Hz.

AlGaN(Si)-based Schottky photodiodes on GaN or AlN nucleation layers showed at all Al compositions a flat spectral response above the bandgap, with a UV/visible contrast in excess of 3 decades. The responsivity of such GaN-based Schottky photodiodes typically was above 50 mA/W. Fast time responses were obtained for these devices, going down to 15 ns. Detectivities of 6.1×10^9 cmHz$^{1/2}$W^{-1} and 1.2×10^9 cmHz$^{1/2}$W^{-1} have been reported respectively in GaN/Au and $Al_{0.22}Ga_{0.78}N$/Au Schottky photodiodes, at –2V bias. The fabrication of GaN-based Schottky photodiodes on ELOG resulted in a very significant improvement of the device performances, with a responsivity of 130 mA/W, a UV/visible contrast over 5 decades, and a high detectivity of 5×10^{11} cmHz$^{1/2}$W^{-1} at –3.4 V bias. AlGaN-based Schottky photodiodes on GaN nucleation layers have finally proved to be able to fit the CIE erythema standard curve, thus opening the door to a new generation of AlGaN-based UV dosimeters.

MSM photodetectors have been fabricated and characterised. The low dark current density indicates the high quality of the Ni/Au Schottky contacts. The devices show a sharp cutoff, with a visible rejection of four to five orders of magnitude at 5 V bias. The photocurrent scales linearly with optical power, for illumination over and below the bandgap, and independently of bias. The RC product of the measurement system limits the time response, the device transit time being far below 10 ns. A NEP* lower than 2 pW/Hz$^{1/2}$ has been obtained in GaN MSM photodetectors, at 28 V bias. From the study of the responsivity of GaN MSM photodiodes we detect a gain mechanism which is only active at bias higher than 2 V, and for excitation over the bandgap. This mechanism is responsible for the superlinear increase of the responsivity with bias observed in AlGaN MSM photodiodes, and also for the enhancement of the UV/visible contrast observed in these devices. Further research is necessary to clarify the physical origin of these phenomena.

Acknowledgements

The authors deeply thank S. Laügt for X-rays measurements, Ph. de Mierry for PDS measurements, M. Passerel for EDS measurements, P. Ruterana for TEM characterisation, M. Leroux for fruitful discussions, and J.P. Faurie for support. This work has been supported by UE Program Environment and Climate, under contract # ENV4-CT97-0539.

References

1. S. Nakamura, *Semicond. Sci. Technol.* **14**, R27 (1999).
2. M.A. Khan, J.N. Kuznia, D.T. Olson, M. Blasingame, and A.R. Bhattarai, *Appl. Phys. Lett.* **63**, 2455 (1993).
3. E. Monroy, F. Calle, C. Angulo, P. Vila, A. Sanz, J.A. Garrido, E. Muñoz, E. Calleja, B. Beaumont, F. Omnes, and P. Gibart, *Appl. Opt.* **37**, 5058 (1998).

4. M. Asif Khan, J.N. Kuznia, D.T. Olson, J.M. Van Hove, M. Blasingame, and L.F. Reitz, *Appl. Phys. Lett.* **60**, 2917 (1992).
5. D. Walker, X. Zhan, A. Saxler, P. Kung, J. Xu, and M. Razeghi, *Appl. Phys. Lett.* **70**, 949 (1997).
6. B.W. Lim, Q.C. Chen, J.Y. Yang, and M.A. Khan, *Appl. Phys. Lett.* **68**, 3761 (1996).
7. E. Monroy, F. Calle, E. Muñoz, F. Omnes, B. Beaumont, and P. Gibart, *J. Electron. Mater.* **28**, 238 (1999).
8. Q. Chen, J.W. Yang, A. Osinsky, S. Gangopadhyay, B.W. Lim, M.Z. Anwar, M.A. Khan, and H. Tempkin, *Appl. Phys. Lett.* **70**, 2277 (1997).
9. A. Osinsky, S. Gangopadhyay, B.W. Lim, M.Z Anzwar, M.A. Khan, D. Kuksenkov, and H. Tempkin, *Appl. Phys. Lett.* **72**, 742 (1998).
10. E. Monroy, F. Calle, E. Muñoz, F. Omnes, P. Gibart, and J.A. Muñoz, *Appl. Phys. Lett.* **73**, 2146 (1998).
11. J.C. Carrano, T. Li, P.A. Grudowski, C.J. Eiting, R.D. Dupuis, and J.C. Campbell, *J. Appl. Phys.* **83**, 6148 (1998).
12. J.C. Carrano, T. Li, D.L. Brown, P.A. Grudowski, C.J. Eiting, R.D. Dupuis, and J.C. Campbell, *Appl. Phys. Lett.* **73**, 2405 (1998).
13. E. Monroy, F. Calle, E. Muñoz, and F. Omnes, *Electron. Lett.* **35**, 240 (1999).
14. J.C. Carrano, T. Li, C.J. Eiting, R.D. Dupuis, and J.C. Campbell, *J. Electron. Mater.* **28**, 325 (1998).
15. E. Monroy, M. Hamilton, D. Walker, P. Kung, F. Sanchez, and M. Razeghi, *Appl. Phys. Lett.* **74**, 1171 (1999).
16. G. Smith, M.J. Estes, T. Dang, A.A. Salvador, Z. Fan, G. Xu, A. Botchkarev, H. Morkoç, and P. Wolf, *Proc. SPIE* **3287**, 198 (1998).
17. G. Parish, S. Keller, P. Kozodoy, J.P. Ibbetson, H. Marchand, P.T. Fini, S.B. Fleischer, S.P. DenBaars, and U.K. Mishra, *Appl. Phys. Lett.* **75**, 247 (1999).
18. J.D. Brown, Z. Yu, S. Harney, J. Boney, J.F. Schetzina, J.D. Benson, K.W. Dang, C. Terrill, T. Nohava, W. Yang, and S. Krishnankutty, *MRS Internet J. Nitride Semicond. Res.* **4**, 9 (1999).
19. M. Morys and D. Berger, *SPIE Proc.* **2049**, 152 (1993).
20. M. Razeghi and A. Rogalski, *J. Appl. Phys.* **79**, 7433 (1996).
21. S. Nakamura, T. Mukai, and M. Senoh, *Jpn. J. Appl. Phys.* **32**, L16 (1993).
22. H. Amano, N. Sawaki, I. Akasaki, and Y. Toyoda, *Appl. Phys. Lett.* **48**, 353 (1986).
23. I. Akasaki, H. Amano, Y. Koide, K. Hiramatsu, and N. Sawaki, *J. Crystal Growth* **98**, 209 (1989).
24. S. Yoshida, S. Misawa, and S. Gonda, *J. Appl. Phys.* **53**, 6844 (1982).
25. H. Angerer, D. Brunner, F. Freundenberg, O. Ambacher, M. Stutzmann, R. Höpler, T. Metzger, E. Born, G. Dollinger, A. Bergmaier, S. Karsch, and H.J. Körner, *Appl. Phys. Lett.* **71**, 1504 (1997).
26. W. Shan, J.W. Ager III, K.M. Yu, W. Walukiewicz, E.E. Haller, M.C. Martin, W.R. McKinney, and W. Yang, *J. Appl. Phys.* **85**, 8505 (1999).
27. T.J. Ochalski, B. Gil, P. Lefebvre, N. Grandjean, M. Leroux, J. Massies, S. Nakamura, and H. Morkoç, *Appl. Phys. Lett.* **74**, 3353 (1999).
28. M.A. Khan, R.A. Skogman, R.G. Schultze, M. Gershenzon, *Appl. Phys. Lett.* **43**, 492 (1983).
29. D.K. Wickenden, C.B. Bargeron, W.A. Bryden, J. Miragliotta, and T.J. Christenmacher, *Appl. Phys. Lett.* **65**, 2024 (1994).
30. S.R. Lee, A.F. Wright, M.H. Crawford, G.A. Petersen, J. Han, and R.M. Biefeld, *Appl. Phys. Lett.* **74**, 3353 (1999).
31. M. Smith, J.Y. Lin, and H.X. Jiang, *Appl. Phys. Lett.* **69**, 2453 (1996).
32. W. Shan, S. Xu, B.D. Little, X.C. Xie, J.J. Song, G.E. Bulman, H.S. Kong, M.T. Leonard, and S. Krishnankutty, *J. Appl. Phys.* **82**, 3158 (1997).
33. B. Beaumont, M. Vaille, T. Boufaden, B. El Jani, and P. Gibart, *J. Cryst. Growth* **170**, 316 (1997).
34. B. Beaumont, S. Haffouz, and P. Gibart, *Appl. Phys. Lett.* **72**, 921 (1998).
35. E. Muñoz, E. Monroy, J.A. Garrido, I. Izpura, F.J. Sánchez, M.A. Sánchez-García, E. Calleja, B. Beaumont, and P. Gibart, *Appl. Phys. Lett.* **71**, 870 (1997).
36. J.A. Garrido, E. Monroy, I. Izpura, and E. Muñoz, *Semicond. Sci. Technol.* **13**, 563 (1998).
37. P.J. Hansen, Y.E. Strausser, A.N. Erickson, E.J. Tarsa, P. Kozodoy, E.G. Brazel, J.P. Ibbetson, U. Mishra, V. Narayanamurti, S.P. DenBaars, and J.S. Speck, *Appl. Phys. Lett.* **72**, 2247 (1998).
38. P. Kung, X. Zhang, D. Walker, A. Saxler, J. Piotrowski, A. Rogalski, and M. Razeghi, *Appl. Phys. Lett.* **67**, 3792 (1995).
39. L.B. Flannery, I. Harrison, D.E. Lacklison, R.I. Dykeman, T.S. Chen, and C.T. Foxon, *Mat. Sci. Eng.* B **50**, 307 (1997).
40. D. Walker, X. Zhan, A. Saxler, P. Kung, J. Xu, and M. Razeghi, *Appl. Phys. Lett.* **70**, 949 (1997).
41. B. Shen, K. Yang, L. Zhan, Z. Chen, Y. Zhou, P. Chen, R. Zhan, Z. Huang, H. Zhou, and Y. Zheng, *Jpn. J. Appl. Phys.* **38**, 767 (1999).
42. J.Z. Li, J.Y. Lin, H.X. Jiang, A. Salvador, A. Botchkarev, and H. Morkoç, *Appl. Phys. Lett.* **69**, 1474 (1996).
43. C. Johnson, J.Y. Lin, H.X. Jiang, M.A. Khan, and C.J. Sun, *Appl. Phys. Lett.* **68**, 1808 (1996).
44. A.Y. Polyakov, N.B. Smirnov, A.V. Govorkov, M.G. Milovidskii, J.M. Redwing, M. Shin, M. Skowronski, D.W. Greve, and R.G. Wilson, *Solid-State Electron.* **42**, 627 (1998).
45. C.H. Qiu, and J.I. Pankove, *Appl. Phys. Lett.* **70**, 1983 (1997).
46. G. Beardie, W.S. Rabinovich, A.E. Wickenden, D.D. Koleske, S.C. Binari, and J.A Freitas, *Appl. Phys. Lett.* **71**, 1092 (1997).
47. H.M. Chen, Y.F. Chen, M.C. Lee, and M.S. Feng, *J. Appl. Phys.* **82**, 899 (1997).
48. C.V. Reddy, K. Balakrishnan, H. Okumura, and S. Yoshida, *Appl. Phys. Lett.* **73**, 244 (1998).
49. P. Kung, X. Zhang, D. Walker, A. Saxler, J. Piotrowski, A. Rogalski, and M. Razeghi, *Appl. Phys. Lett.* **67**, 3792 (1995).
50. F. Binet, J.Y. Duboz, E. Rosencher, F. Scholz, and V. Härle, *Appl. Phys. Lett.* **69**, 1202 (1996).
51. J.A. Garrido, E. Monroy, I. Izpura, and E. Muñoz, *Semicond. Sci. Technol.* **13**, 563 (1998).
52. C.H. Qiu, C. Hoggatt, W. Melton, M. W. Leksono, and J.I. Pankove, *Appl. Phys. Lett.* **66**, 2712 (1995).
53. O.H. Nam, M.D. Bremser, T. Zheleva, and R.F. Davis, *Appl. Phys. Lett.* **71**, 2638 (1997).

 © 2000 COSiW SEP, Warsaw

54. A. Usui, H. Sunakawa, A. Sakai, and A. Yamaguchi, *Jpn. J. Appl. Phys.* **36**, L899 (1997).
55. E. Monroy, F. Calle, E. Muñoz, B. Beaumont, F. Omnes, and P. Gibart, *Electron. Lett.* **35**, 1488 (1999).
56. A.F. McKinley and B.L. Diffey, *CIE Journal* **6**, 17 (1987).
57. F.R. De Gruji and J.C. Van der Leun, *Health Phys.* **67**, 314 (1994).
58. R.B. Setlow, *Proc. Natl. Acad. Sci. USA* **71**, 3363 (1974).
59. L.W. Jones and B. Kok, *Plant Physiol.* **41**, 1037 (1966).
60. E. Muñoz, E. Monroy, F. Calle, M.A. Sánchez, E. Calleja, F. Omnes, P. Gibart, F. Jaque, and I. Aguirre de Cárcer, *SPIE Proc.* **3629**, 200 (1999).
61. E. Muñoz, E. Monroy, F. Calle, F. Omnes, and P. Gibart, *J. Geophys. Res.* (to be published).
62. P. Bhattacharya, *Semiconductor Optoelectronic Devices*, Prentice Hall, New Jersey, 1994.
63. S.M. Sze, *Physics of Semiconductor Devices*, Wiley, New York, 1981.
64. S.M. Sze, D.J. Coleman, and A. Loya, *Solid-State Electron.* 14, 1209 (1971).
65. E. Monroy, F. Calle, E. Muñoz, and F. Omnes, *Physica Status Solidi* **A** (to be published).
66. E. Monroy, F. Calle, E. Muñoz, and F. Omnes, *Appl. Phys. Lett.* **74**, 3401 (1999).
67. D. Walker, E. Monroy, P. Kung, J. Wu, M. Hammilton, F.J. Sánchez, J. Diaz, and M. Razeghi, *Appl. Phys. Lett.* **74**, 762 (1999).
68. S.F. Soares, *Jpn. J. Appl. Phys.* **31**, 210 (1992).
69. M. Klingenstein and J. Khul, *Solid-State Electron.* **37**, 333 (1994).
70. J. Burm and L.F. Eastman, *IEEE Photonics Technol. Lett.* **8**, 113 (1996).